A 3D TOMOGRAPHIC MODEL OF SOUTH CENTRAL ASIA BASED ON Pn TRAVEL TIMES FROM GT EVENTS

Christopher J. Young[1], Sanford Ballard[1], James R. Hipp[1], Marcus C. Chang[1], Glenn T. Barker[1], Michael L. Begnaud[2], W. Scott Phillips[2], Lee K. Steck[2], and Charlotte A. Rowe[2]

Sandia National Laboratories[1] and Los Alamos National Laboratory[2]

Sponsored by National Nuclear Security Administration

Contract Nos. DE-AC04-94AL8500 and DE-AC52-06NA25396.

ABSTRACT

Increasingly, nuclear explosion monitoring is focusing on detection, location, and identification of small events recorded at regional distances. Because Earth structure is highly variable on regional scales, locating events accurately at these distances requires the use of region-specific models to provide accurate travel times. Improved results have been achieved with composites of 1D models and with approximate 3D models with simplified upper mantle structures, but both approaches introduce nonphysical boundaries that are problematic for operational monitoring use. Ultimately, what is needed is a true, seamless 3D model of the Earth.

Towards that goal, we have developed a 3D tomographic model of the P velocity of the crust and upper mantle for the region of southcentral Asia centered around the Tibetan Plateau. Our model is derived from almost 140,000 Pn picks for more than 5300 events recorded at 563 stations from a Ground Truth (GT) dataset assembled by Los Alamos National Laboratory (LANL). Our starting model is the a priori model of East Asia developed by LANL, which is based on various global and regional studies. The topmost layers come from the Laske and Masters global sedimentary model from 1997. As our dataset lacks the resolution to improve this sedimentary portion of our model, we fix the velocity and depth of these layers, as well as the depths of the major mantle discontinuities (Moho, 410 km, 660 km). We invert for P velocities from the crust down through the upper mantle, along with source and receiver terms to account for the effects of event mislocation and fine-scale structure near the receiver not accounted for in the crustal model. Forward calculations are made using our own implementation of the Um and Thurber ray pseudo-bending approach (Ballard, 2008, these Proceedings) with full enforcement of Snell's Law in 3D at the major discontinuities. Because large portions of the model are underconstrained, we apply both damping and regularization to force the inversion to update the initial model only where good data coverage is available. We validate the model by performing several inversions with random portions of the dataset omitted and then testing the predictive capability of the model against those portions compared with AK135. We test the location performance of the model by relocating the GT events using our model and using AK135.

Report Documentation Page

Form Approved
OMB No. 0704-0188

1. REPORT DATE	2. REPORT TYPE	3. DATES COVERED
SEP 2008		**00-00-2008 to 00-00-2008**

4. TITLE AND SUBTITLE	5a. CONTRACT NUMBER
A 3D Tomographic Model of South Central Asia Based on Pn Travel Times from GT Events	5b. GRANT NUMBER
	5c. PROGRAM ELEMENT NUMBER
6. AUTHOR(S)	5d. PROJECT NUMBER
	5e. TASK NUMBER
	5f. WORK UNIT NUMBER
7. PERFORMING ORGANIZATION NAME(S) AND ADDRESS(ES) **Sandia National Laboratory,PO Box 969,Livermore,CA,94551-0969**	8. PERFORMING ORGANIZATION REPORT NUMBER
9. SPONSORING/MONITORING AGENCY NAME(S) AND ADDRESS(ES)	10. SPONSOR/MONITOR'S ACRONYM(S)
	11. SPONSOR/MONITOR'S REPORT NUMBER(S)

12. DISTRIBUTION/AVAILABILITY STATEMENT
Approved for public release; distribution unlimited

13. SUPPLEMENTARY NOTES
Proceedings of the 30th Monitoring Research Review: Ground-Based Nuclear Explosion Monitoring Technologies, 23-25 Sep 2008, Portsmouth, VA sponsored by the National Nuclear Security Administration (NNSA) and the Air Force Research Laboratory (AFRL)

14. ABSTRACT
see report

15. SUBJECT TERMS

16. SECURITY CLASSIFICATION OF:			17. LIMITATION OF ABSTRACT	18. NUMBER OF PAGES	19a. NAME OF RESPONSIBLE PERSON
a. REPORT **unclassified**	b. ABSTRACT **unclassified**	c. THIS PAGE **unclassified**	**Same as Report (SAR)**	**9**	

OBJECTIVES

Our goal is to better predict Pn travel times for an area of south central Asia centered around the Tibetan Plateau. This is an area of high monitoring interest, as it encompasses the Indian, Pakistani, and Chinese test sites, as well as the former Soviet test site at Shagan River (now in Kazakhstan). It also spans several other countries that could be candidates for nuclear testing. Thus, locating events accurately in this region is tremendously important for tracking treaty compliance and nuclear weapon proliferation. To accomplish our goal, we have developed a three-dimensional (3D) P velocity model of the crust and upper mantle in this region. This is one of the most tectonically complex areas on the Earth, due to the collision of the Indian and Asian continents, which has led to the highest mountain ranges in the world, as well as the thickest crust and lithosphere.

RESEARCH ACCOMPLISHED

Dataset

Our data are drawn from an East Asia GT dataset collected over the past several years by Ground-Based Nuclear Explosion Monitoring Research and Development (GNEMRD) researchers at LANL. Considerable effort has gone into the collection of this dataset to draw on all possible sources of event catalogs for this region, and then to carefully screen them. Events are drawn from global catalogs from the NEIC (National Earthquake Information Center), and ISC (International Seismological Centre), as well as from various regional catalogs including the Annual Bulletin of Chinese Earthquakes (ABCE) (Lee et al., 2002). All events in the LANL GT set are assigned a GT level based on the Bondár criteria (Bondár et al., 2004), and for this project, only events with GT levels of 25 km or better were used. For each of these events, picks from the various catalogs were merged, removing redundant and/or outlier arrivals based on a preferred catalog hierarchy. Events without a priori GT information were relocated with the merged arrival set, comparing the results to the Bondár criteria (Begnaud et al., 2006). To focus on P velocity in the upper mantle, we chose to use only Pn phases and have limited source to receiver path lengths to be 25 degrees or less. This resulted in approximately 110,000 Pn picks for more than 5300 events recorded at 563 stations (Figure 1).

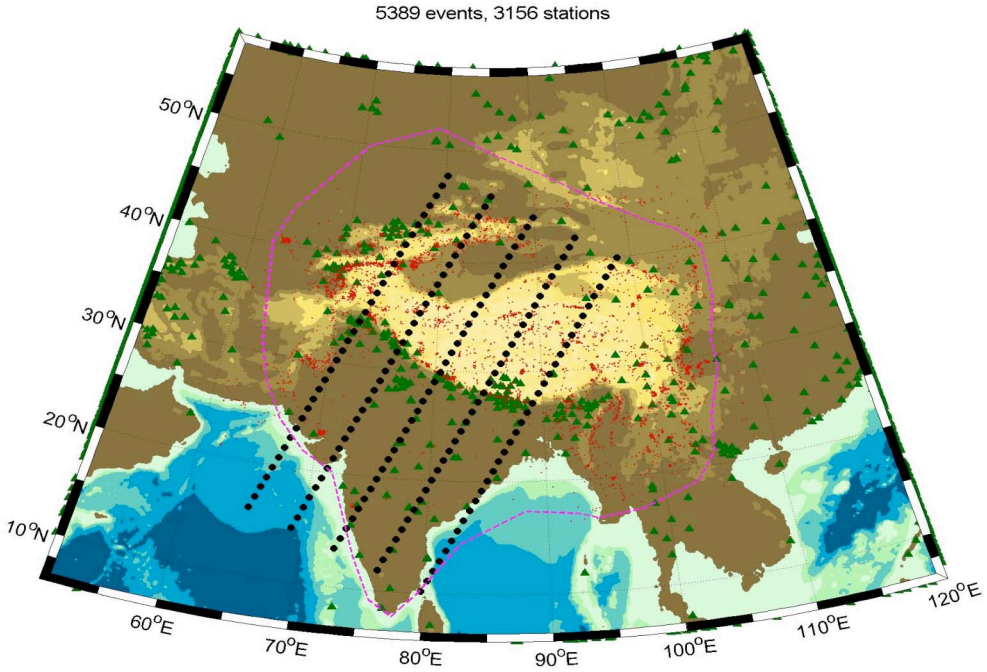

Figure 1. Map showing the seismic events (red circles) and stations (green triangles) used in this study. The magenta dashed line shows the extent of the tomographic model we invert for, while the lines of black circles show the positions of cross sections through our model presented later.

Model Structure

One of the areas in which we believe our model is an improvement over many of the previous tomographic models of the region is in the structure of the model. Many previous studies have used geographic grids that are regularly spaced in latitude and longitude. These types of grids are easy to construct and to use for interpolation (locating neighbor node positions within them is trivial), but they are inefficient because they compress northward as the longitude meridians converge. We instead use a grid that is truly equally spaced, regardless of latitude, as is shown in Figure 2. This grid is derived by progressive subdivision of an icosahedron with 12 nodes to a set of nodes with the desired spacing (see Ballard et al., 2008a, these Proceedings, for more details). As with a regular geographic grid, values at intermediate positions are found by interpolation of values at the neighbor nodes, but for this type of grid the neighbor nodes are found by a standard walking triangle search. To avoid the complications of dealing with ray paths that cross in and out of our model, we use a global grid, but the grid spacing is variable, being 1 degree in Eurasia and 2 degrees everywhere else in the world. The radial structure at each of these geographic node positions is represented with a standard set of layers that extend from the surface of the Earth to the center of the Earth: sediments, upper crust, mid-crust, lower crust, uppermost mantle, etc. The thicknesses (layers can pinch out), top and bottom depths, and top and bottom velocities of each of these layers can all change with geographic position, though we do assume that the velocity within a layer is fit by a linear gradient between the top and bottom values. Values at intermediate positions within layers are interpolated. Our model structure is described in more detail in the companion presentation by Ballard et al. (2008a, these Proceedings).

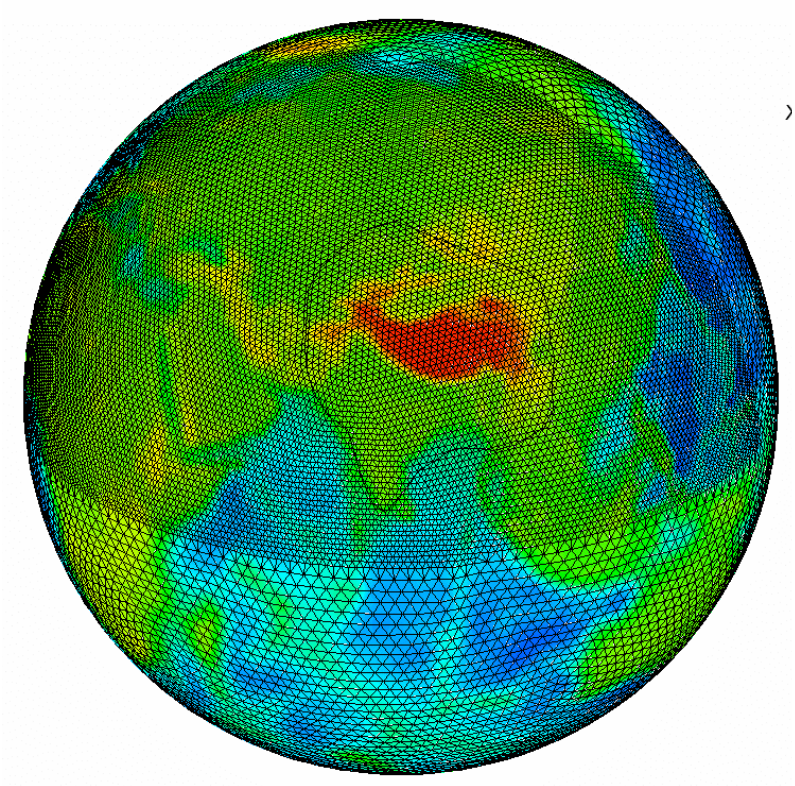

Figure 2. Geographic grid for the tomographic model. Color is proportional to topography (red is high, green is medium, and blue is low). Each node marks the position of a layered profile extending from the surface to the center of the Earth. The black line around the Indian subcontinent and the Tibetan Plateau shows the portion of the overall model that will be updated by our tomographic inversion.

Starting Model

As mentioned above, even though our goal is improved structure for a limited region of southern Asia, we have found it to be more straightforward to work with a global model. For a background, we use the crustal structure from the Laske, Master, and Reif Crust 2.0 model (Laske et al., 2008) on top of an AK135 mantle. For Europe, North Africa, and Asia, we use the a priori GNEMRD Unified Model created collaboratively by LANL and Lawrence Livermore National Laboratory (LLNL) (Begnaud et al., 2004; Pasyanos et al., 2004). This model has been shown to provide better Pn travel times than AK135 for Eurasia and North Africa (Flanagan et al., 2007), but not for southern Asia (Young et al., 2008), hence our motivation for this study. Shallow sedimentary layers are taken from Crust 2.0, while the deeper crustal layers are taken from various focused regional studies. The model also includes upper mantle structure from the 3SMAC model (Nataf and Ricard, 2004), but we choose not to use this because it is not based on seismic data. Instead, we use AK135 mantle structure.

Limitations on the Inversion

Based on the ray paths connecting our sources and receivers, we constructed the polygon shown in Figures 1 and 2 to limit the extent of our inversion. Only the velocities at the nodes within this polygon were updated. Further, we do not allow either the thicknesses or the depths of layers to change: only P velocities at the tops and bottoms of layers can be modified. We only include ray paths in the inversion that have 3/4 or more of their path lengths lying within our polygon. For such rays, observed times are always reduced by the travel time for the portion of the path external to the polygon before inversion. Because we are using Pn data only, we limit our inversion to rays that turn below the Moho but above the 410 km discontinuity. Hence, our inversion is limited to the crust and the portion of the upper mantle above the transition zone.

Inversion Formulation

Our inversion minimizes the travel time residuals formed by subtracting predicted Pn travel times from observed travel times. We assume that the travel time residual along a path from a source i to a receiver j can be calculated by multiplying the required slowness perturbations along the path by the lengths of the segments along the path, i.e.,

$$\Delta t_{ij} = \sum_{\ell} d_{\ell} * \Delta s_{\ell} \,, \tag{1}$$

where d_{ℓ} is the length of a path along the lth segment and Δs_{ℓ} is the slowness perturbation along that segment. With perfect data and perfect coverage of the entire model, this equation could be inverted directly to solve for the slowness perturbations (and hence the velocity structure). However, the data are never perfect, nor is the coverage, so a best model is solved for iteratively using a least-squares minimization of the residuals.

In tomographic inversions where the model is structured as a set of blocks, it is the path length through those blocks that provide the weights to be multiplied by the slowness perturbations to get the residuals. Because our model is represented by a set of nodes instead of blocks, the formulation is slightly different. We divide each path length into equal length subsegments 10 km long, then for each subsegment, we interpolate from the surrounding nodes to get the appropriate slowness to multiply times the subsegment length. Hence, in our formulation, we are solving for the slowness perturbation at the nodes, and the coefficients multiplying each of the node slowness perturbations are a combination of the path subsegment lengths and the weights of the nodes used for the interpolation. Because our data have noise, we cannot find a model that gives a zero residual everywhere but instead seek to minimize the squared residual:

$$\varepsilon = \left\| A\Delta s - \Delta t \right\|^2, \tag{2}$$

where A is an *n* (number of observations) by *m* (number of nodes) matrix of node coefficients, Δs is an *m* by 1 array of slowness perturbations, and Δt is an n by 1 array of travel-time residuals.

Because portions of the model are under-constrained, we impose damping. In addition, we add horizontal and vertical smoothing (regularization) to produce models that are consistent with our geophysical intuition. Thus, the overall equation we invert is of this form:

$$\varepsilon = \left\| A\Delta s - \Delta t \right\|^2 + \lambda \left\| \Delta s \right\|^2 + \gamma \left\| L\Delta s \right\|^2 , \quad (3)$$

where λ is the damping coefficient, γ is the smoothing factor, and L is the matrix of smoothing operators. To control the slowness adjustments in regions of the model where sampling is very poor, we use separate damping coefficients for each node slowness perturbation and make the damping coefficient for each inversely proportional to the ray coefficients, i.e., nodes with very little path sampling are highly damped, while those with high path sampling are damped very little.

Travel-Time Prediction Calculation and Ray Paths

Another area in which we believe this study improves over previous tomographic studies of the area is in our calculation of travel times and ray paths. For each iterative model, beginning with the starting model, we calculate true 3D ray paths using our own implementation of the Um and Thurber (1987) pseudo-bending methodology. Our implementation requires rays to honor Snell's Law at discontinuities (in this case the Moho), and it also avoids local minima by solving for a ray (refracted, diffracted, or reflected) in each layer, then finding the first refracting arrival. We have shown our implementation to be highly accurate (Young et al., 2008), but also computationally expensive, so we have designed a distributed computing framework to allow a set of rays to be run simultaneously on multiple processors. For our calculations for this model, we used a set of nine 16-processor PC-architecture machines for a total of 144 processors. For more on the ray bending algorithm implementation, we refer the reader to the companion paper by Ballard et al. (2008b).

Travel-Time Prediction Improvement

The ultimate goal of this project is to develop a model that can provide better Pn travel time predictions for our area. Our model shows clear improvements over the AK135 model for our dataset. Figure 3 shows mean and standard deviations of the observed minus prediction residuals for both models.

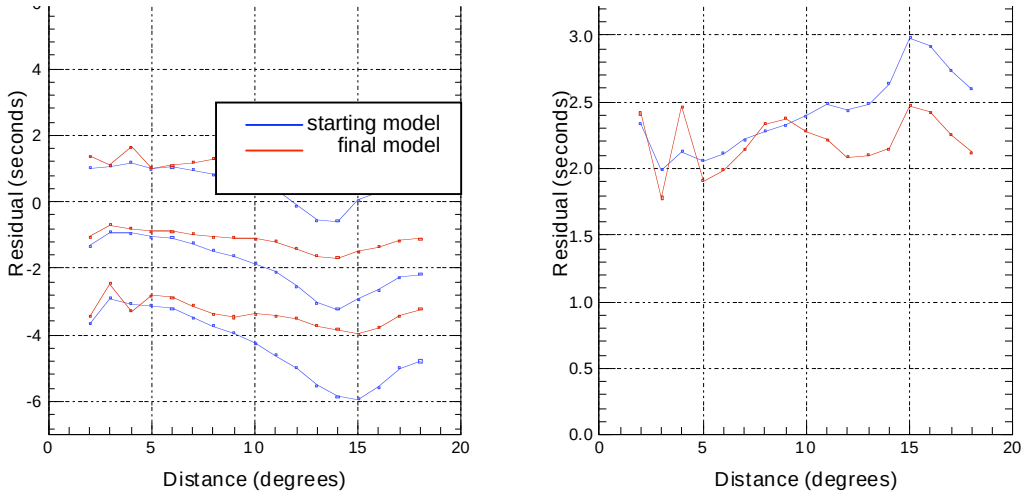

Figure 3. (left) One degree station to event distance bins of mean plus and minus one standard deviation for starting model (red) and final model. (right) One degree station to event distance bins of standard deviation.

The means of the residuals at all distances are negative for AK135, indicating that the data require a faster model. Further, the standard deviations are large (over 2 seconds), suggesting that there is considerable lateral heterogeneity in the region.

For our model, the overall RMS of the residuals has been reduced from 3.2 seconds to 2.5 seconds, an improvement of 22%. This suggests that we are modeling a substantial portion of the lateral heterogeneity in the region. The bulk of the improvement comes beyond 8 degrees, suggesting that it is the changes in the upper mantle portion of our model that are the most important. Our model decreases the bias, especially beyond 8 degrees, but does not remove it. We believe that the reason for this is that our damping coefficients were too strong, hence the model was unable to move far enough away from the starting model. In subsequent versions of the model, we plan to vary the damping coefficients to see if we can remove the bias entirely.

Discussion of the Tomographic Model

Figure 4 shows percent velocity changes from the staring model at the bottom of the lowermost crustal layer, at the top of the uppermost mantle layer, at 100 km, and at 200 km. To help interpret these pictures, at each depth we also show a map of the node ray hit count at each depth. Generally ray hit counts are good across the model for all depths, but there are lower hit counts at the edges of the model, especially in the crust where the ray paths are much more vertical than in the mantle.

Beginning with the shallowest structure and working downwards, we can see that overall the adjustments to the velocity at the base of the crust are much less than in the mantle. This suggests that the crustal portion of our starting model is doing a good job of fitting the data, as expected. Still, our results suggest that the crustal velocities beneath the Tibetan Plateau are lower than in the starting model, and that the velocities to the NW and SE of the plateau need to be higher to match the observations.

The strongest velocity changes are seen at 100-km depth, and they are predominantly velocity increases, which is consistent with the negative bias of the starting model seen in Figure 3. Velocities have been increased by 2% and greater throughout most of the region, with the exception of low-velocity regions near the Tarim Basin and in the southeast part of China. Both the positive and negative features seem to extend upward to the Moho and downward to 200 km, though not as strongly. Depth extent can be better assessed with the vertical cross sections shown in Figure 5 for the profiles shown in Figure 1. We can see a high-velocity region extending from the Indian subcontinent underneath the Tibetan Plateau, then being sharply truncated by low-velocity material at the Tarim Basin for slices that cross that basin farther to the east. Both these high and low-velocity anomalies extend from the top of the mantle down to at least 200 km. How much deeper they extend is not clear because of our poor ray coverage at depth.

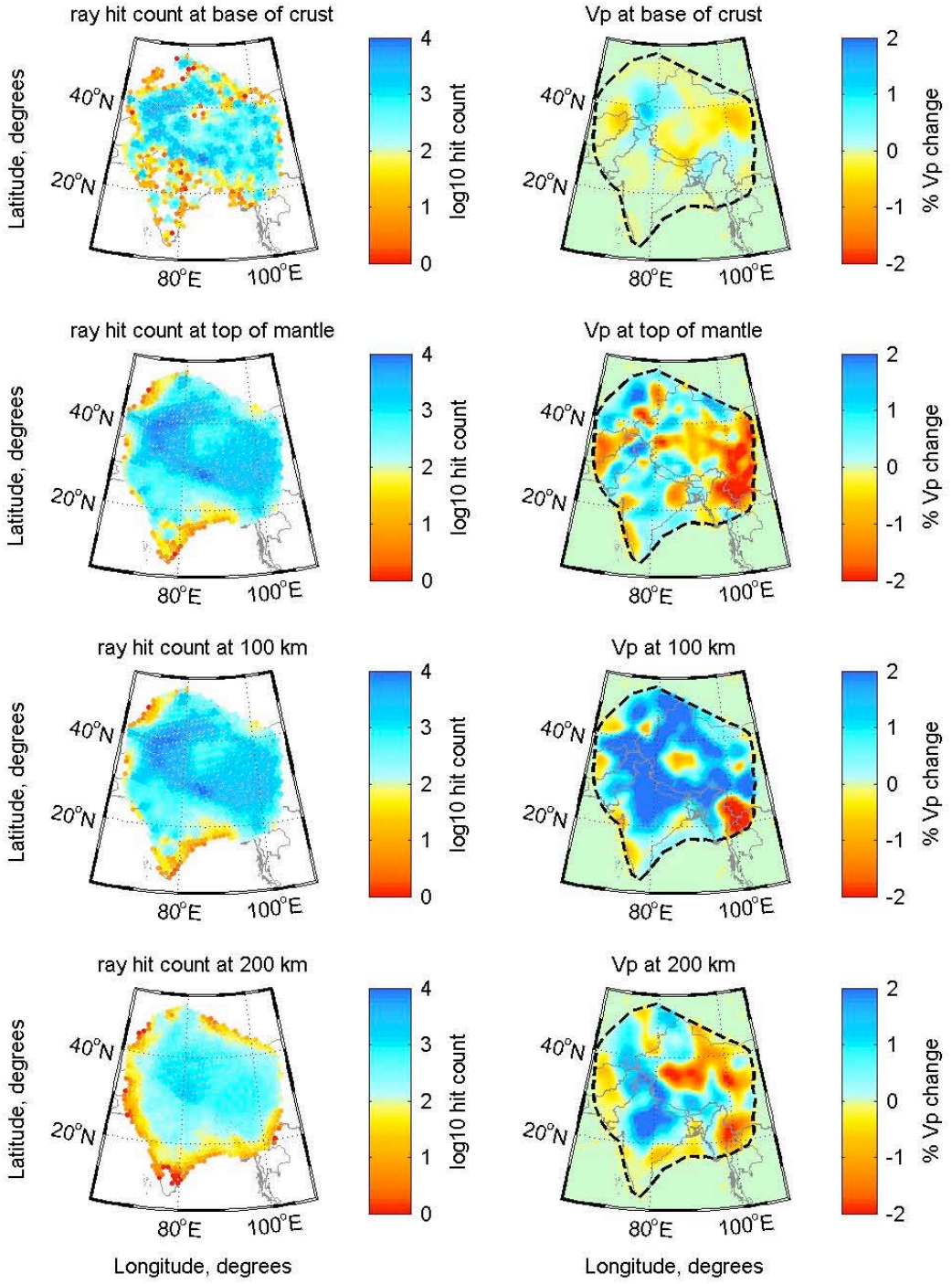

Figure 4. (left side, top to bottom) Log10 ray hit counts for nodes at the base of the crust, the top of the mantle, the top of the 100-km-depth layer, and the top of the 200-km-depth layer. (right side, top to bottom) Percent P velocity change from starting model for the same nodes and depths.

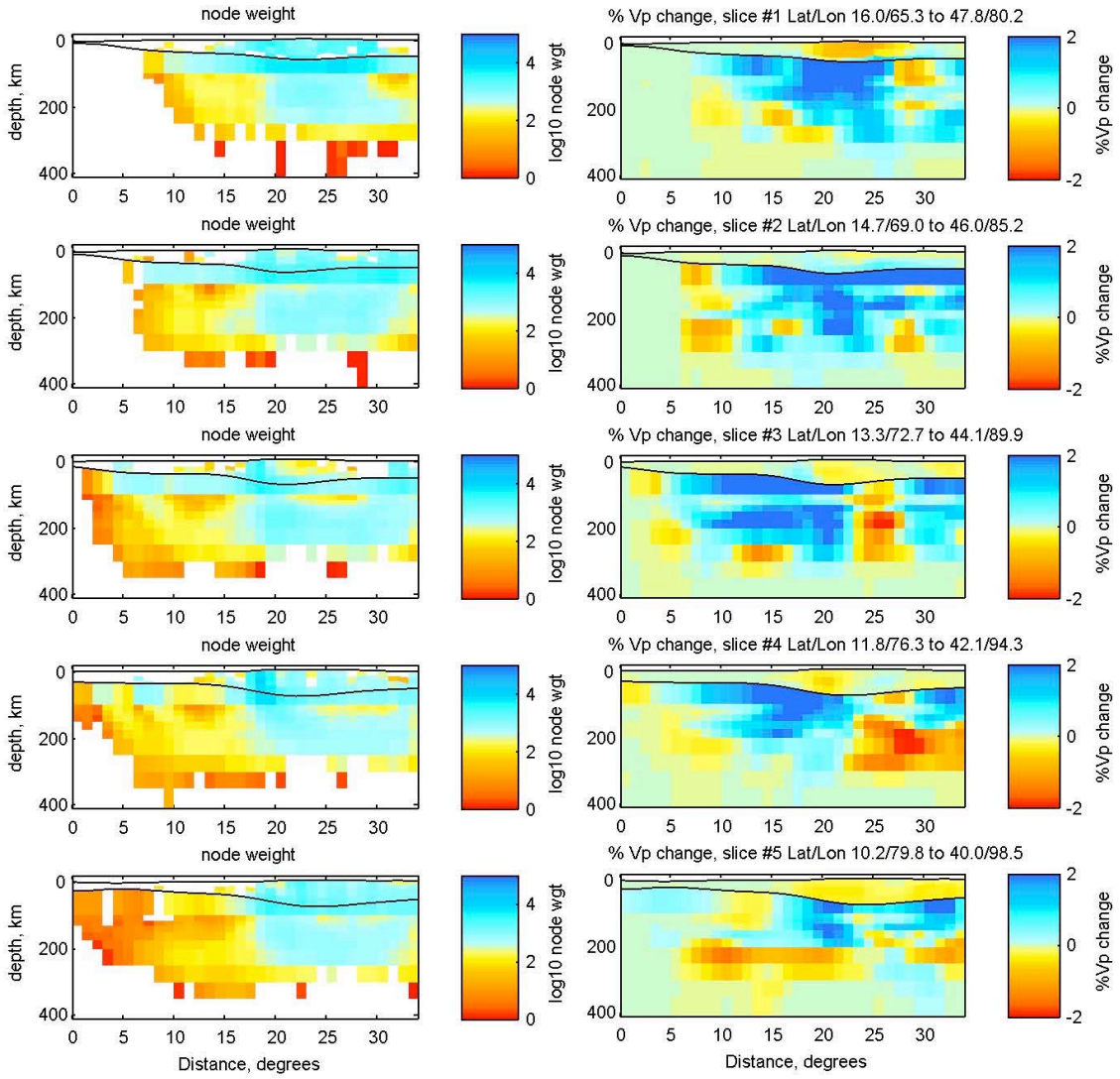

Figure 5. (left side, top to bottom) Log10 ray hit counts for cross section slices shown in Figure 1. (right side, top to bottom) Percent P velocity change from the starting model for the same cross sections.

CONCLUSIONS AND RECOMMENDATIONS

We have developed a 3D model of the P velocity structure of the crust and upper mantle for a limited region of south central Asia. Our approach differs from previous efforts in several important ways. First, we utilize only high-quality GT data, collected by LANL GNEMRD researchers over the past several years. Second, our model is represented geographically with a grid of truly equally spaced nodes, and radially with a set of standard layers with variable properties. Third, we trace rays and calculate travel times using a 3D pseudo-bending approach that enforces Snell's law across discontinuities. The resulting model provides a 22% improvement in RMS travel-time residual over our starting model, which is taken from the LANL/LLNL a priori unified geophysical model that encompasses our region. Overall, our model is faster than the starting model, hence reducing the negative bias in residuals, but our model still has a negative bias, probably because damping is too strong. In future versions of the model, we plan to experiment with changing damping and regularization parameters to improve our model further.

REFERENCES

Ballard, S., C. Young, J. Hipp, G. Barker, and M. Chang (2007). Computation of travel time through 3D velocity models for applications in real-time, global seismic event monitoring, *EOS Trans. AGU*, Fall Meet. Suppl.

Ballard, S., Hipp, J., and C. Young (2008a). Robust, extensible representation of complex earth models for use in seismological software systems, these Proceedings.

Ballard, S., Young, C., Hipp, J., G. Barker, and M. Chang (2008b). Implementation of a pseudo-bending seismic travel time calculator in a distributed computing environment, these Proceedings.

Begnaud, M. L., C. A. Rowe, and L. K. Steck (2004). Validating three-dimensional velocity models in China and East-Asia for use in regional seismic event location, *EOS Trans. AGU*, Fall Meet. Suppl.

Begnaud, M. L., L. K. Steck, and C. A. Rowe (2006). Improving seismic event locations in Asia by using catalog-scale empirical travel time correction surfaces, *EOS Trans. AGU* 87(52), Fall Meet. Suppl., Abstract T51D-1550.

Bondár, I., S. C. Myers, E. R. Engdahl, and E. A. Bergman (2004). Epicentre accuracy based on seismic network criteria, *Geophys. J. Int.* 156: 483–496.

Flanagan, M. P., S. C. Myers, and K. D. Koper (2007). Regional travel-time uncertainty and seismic location improvement using a three-dimensional a priori velocity model, *Bull. Seism. Soc. Am.* 97: 804–825.

Laske, G., G. Masters, and C. Reif (2008). Crust2.0: A new global crustal model at 2x2 degrees, http://mahi.ucsd.edu/Gabi/rem.dir/crust/crust2.html.

Lee, W. H. K., H. Kanamori, P. C. Jennings and C. Kissling (Eds.) (2002). *International Handbook of Earthquake and Engineering Seismology* (CD-ROM), Elsevier, New York.

Nataf, H. C. and Y. Ricard (2004). 3SMAC: An a priori tomographic model of the upper mantle based on geophysical modeling, *Phys. Earth Planet. Int.* 95: 101–122.

Pasyanos, M. E., W. R. Walter, M. P. Flanagan, P. Goldstein, and J. Bhattacharyya (2004). Building and testing an a priori geophysical model for Western Eurasia and North Africa, *Pure Appl. Geophys.* 161: 234–281.

Um, J. and C. Thurber (1987). A fast algorithm for two-point seismic ray tracing, *Bull. Seism. Soc. Am.* 77: 972–986.

Young, C. J., S. Ballard, G .T. Barker, M. L. Begnaud, C. A. Rowe, W. S. Phillips, and L. K. Steck (2008). Validating P wave travel times for a 3D model of East Asia using a pseudo-bending travel time calculation and a large GT data set, SSA 2008 Meeting, *Seismo. Res. Lett.* 79: 305.